RSC Advances

PAPER

View Article Online
View Journal | View Issue

Cite this: RSC Adv., 2017, 7, 12074

Ab initio conical intersections for the Si(^{1}D) + H_2 reaction system: a lowest five singlet states study†

Yanan Wu,[ab] Chunfang Zhang[ab] and Haitao Ma*[a]

Conical intersection (CI) play a key role in the non-adiabatic processes and the geometric phase (GP) effect associated with CI have a significant influence on the quantum reactive scattering and bound-state calculations. In this work, the CIs and the GP effects associated with the CIs of the Si(^{1}D) + H_2 system are investigated using the internally contracted multireference configuration intersection method for the first time. The seams of the CIs (at the linear H–Si–H geometries, linear Si–H–H geometries and C_{2v} geometries) among the lowest five singlet states relative to the Si(^{1}D) + H_2 reaction system are searched systematically. The properties of minimum energy crossing points (MECPs) of these intersection seams are determined, the topographies of the potential energy surfaces in the branching spaces of MECPs and the GP effects associated with the CIs are discussed.

Received 23rd January 2017
Accepted 14th February 2017

DOI: 10.1039/c7ra01021d

rsc.li/rsc-advances

1 Introduction

Silylene, SiH_2, the prototype radical in silylene family, plays an important role in the organic silicon chemistry,[1–3] and it is postulated as a reactive intermediate in the manufacturing process of amorphous silicon films by chemical vapor deposition.[4–7] The studies of SiH_2 started as early as 1967, when Dubois and co-workers observed electronic absorption spectra belonging to the $\tilde{X}^1A_1$–$\tilde{A}^1B_1$ transition of this radical for the first time.[8] It was not ascertained that whether the lower $^1A_1$ state of the observed transition was the ground state or there was a lower-lying triplet state, as in CH_2, would be the ground state until Milligan and Wirsam's work confirmed that the lower state of the previously observed electronic transition of singlet SiH_2, is the ground state[9,10] and Apeloig and co-workers explained why CH_2 is a ground state triplet while SiH_2 is a ground state singlet.[11] Most of the studies about this radical concentrated on the $\tilde{X}^1A_1$ and $\tilde{A}^1B_1$ states. Dubois and co-workers measured the absorption spectrum of the $\tilde{X}^1A_1$–$\tilde{A}^1B_1$ transition of SiH_2 and pointed out the existence of a lot of strong and erratic rotational perturbations.[8,12,13] The anomalous rotational perturbations were interpreted as the combined effects of the Renner–Teller coupling between the two singlet states and the spin–orbit coupling with the lowest triplet state,[13,14] and the large amplitude motion of the bending vibration ν_2.[14,15] It was reported that fluorescence lifetime of SiH_2 in the $\tilde{A}^1B_1$ state widely vary for each rovibronic level,[16,17] and this was interpreted in terms of mixing with adjacent levels of the $\tilde{a}^3B_1$ state,[18] and the predissociation to Si(^{3}P) + H_2.[16,19,20] Ishikawa *et al.* observed the stimulated emission pumping spectroscopy of the $\tilde{A}^1B_1$–$\tilde{X}^1A_1$ transition and obtained information about the $\tilde{a}^3B_1$ state through the spin–orbit interaction.[21] Yurchenko *et al.* first made an *ab initio* calculation of the potential energy surfaces (PESs) for the $\tilde{X}^1A_1$ and $\tilde{A}^1B_1$ states, and they calculated the rovibronic energies of the two states using this *ab initio* PESs.[22] Researches that refer to higher electronic states than the $\tilde{A}^1B_1$ state were much fewer. The $\tilde{B}^1A_1$ state of SiH_2 and SiD_2 radicals was observed for the first time in 2005.[23] Before long, Tokue *et al.* evaluated the transition probabilities of the $\tilde{X}^1A_1$–$\tilde{A}^1B_1$ and $\tilde{A}^1B_1$–$\tilde{B}^1A_1$ systems of SiH_2 and SiD_2,[24] and they also investigated the photodissociation process of $SiH_2(\tilde{A}^1B_1) \rightarrow SiH_2(\tilde{B}^1A_1) \rightarrow$ Si(^{1}D) + H_2.[25]

Conical intersections (CIs),[26] not isolated geometries but form a seam,[27] are widespread in polyatomic systems and play a key role in non-adiabatic processes,[28,29] such as charge-transfer reaction,[30,31] nonradiative transition, and electronic quenching. At a CI, the Born–Oppenheimer approximation stipulating that electronic and nuclear motions are separable breaks down.[32] Therefore, molecular systems which exhibit such topologies rapidly switch between electronic states through the funnel of the CI.[33] Recently, many theoretical and experimental studies about the typical non-adiabatic process associated with CIs, such as electron transfer, isomerization, photoinduced unimolecular decay, and radiationless relaxation of the excited electronic state, have provided lots of valuable new insights into the nature of CIs.[30,34–41] There have been some *ab initio* studies about the CIs in triatomic molecules.[42–52] While, the detailed studies of the CIs or PES intersections of the Si(^{1}D) + H_2 system have never been reported.

[a]Beijing National Laboratory for Molecular Sciences, Institute of Chemistry, Chinese Academy of Sciences, Beijing 100190, China. E-mail: mht@iccas.ac.cn

[b]University of Chinese Academy of Sciences, Beijing 100049, China

† Electronic supplementary information (ESI) available: Seam lines of the conical intersections and three dimension representation of the geometric phase effect associated with the conical intersection in the Si(^{1}D) + H_2 system. See DOI: 10.1039/c7ra01021d

Geometric phases (GP) or Berry phases[53] are ubiquitous in physics and chemistry, and some of the most fascinating phenomena in condensed matter science such as topological insulators,[54] ferroelectrics,[55] the Aharonov–Bohm effect,[56] and it is regarded as the signature property and associated non-adiabatic effect of CIs in molecules.[57,58] GP may arise when the Hamiltonian of a system depends on a set of parameters R. Consider a physical system described by a Hamiltonian that depends on time through a set of parameters, denoted by $\boldsymbol{R} = (R_1, R_2, \ldots)$, *i.e.*,

$$H = H(R),\ R = R(t). \tag{1}$$

We are interested in the adiabatic evolution of the system as $R(t)$ moves slowly along a path C in the parameter space. For this purpose, it is useful to introduce an instantaneous orthonormal basis from the eigenstates of $H(\boldsymbol{R})$ at each value of the parameter $\boldsymbol{R}$, *i.e.*,

$$H(R)|n(R)\rangle = \varepsilon_n(R)|n(R)\rangle. \tag{2}$$

However, eqn (2) alone does not completely determine the basis function $|n(R)\rangle$, it still allows an arbitrary R-dependent phase factor of $|n(R)\rangle$. One can make a phase choice, also known as a gauge, to remove this arbitrariness. Here we require that the phase of the basis function is smooth and single valued along the path C in the parameter space.

According to the quantum adiabatic theorem, the solution of the time-dependent Schrödinger equation is written as

$$|\psi_n(t)\rangle = \mathrm{e}^{i\gamma_n(t)} \exp\left[-\frac{i}{\hbar}\int_0^t \mathrm{d}t'\varepsilon_n\big(R(t')\big)\right]|n(R(t))\rangle, \tag{3}$$

where the second exponential is known as the dynamical phase factor. Inserting eqn (3) into the time-dependent Schrödinger equation

$$i\hbar\frac{\partial}{\partial t}|\psi_n(t)\rangle = H(R(t))|\psi_n(t)\rangle \tag{4}$$

and multiplying it from the left by $|\psi_n(t)\rangle$, one finds that $\gamma_n(t)$ can be expressed as a path integral in the parameter space

$$\gamma_n = \int_C \mathrm{d}R\cdot A_n(R), \tag{5}$$

where $_n(R)$ is a vector-valued function

$$A_n(R) = i\langle n(R)\Big|\frac{\partial}{\partial R}\Big|n(R)\rangle \tag{6}$$

This vector $_n(R)$ is called the Berry connection or the Berry vector potential. Eqn (5) shows that, in addition to the dynamical phase, the quantum state will acquire an additional phase γ_n during the adiabatic evolution. Therefore, for a closed path, γ_n becomes a gauge-invariant physical quantity, known as the Berry phase or geometric phase in general; it is given by

$$\gamma_n = \oint_C \mathrm{d}R\cdot A_n(R). \tag{7}$$

By virtue of the above derivation of GP,[55] the GP associated with a CI comes down to the statement that the real adiabatic electronic wave function may acquire a phase which leads to a flip of sign when nuclear configuration traverse a closed path encircling a CI.[59,60] Since the total molecular wave function has to remain single-valued, a compensating sign change must occur in the nuclear motion wave function. In order to investigate the GP effects in chemical reaction dynamics and the energy levels of bound-state molecules, the compensating sign of the nuclear motion wave function must be included in quantum reactive scattering and bound-state calculations. The GP effects on the energy levels of bound-state molecules have been well understood,[60–62] it has been shown that they are pronounced on the bound-state spectrum of HO_2, Na_3, and N_3.[62–64] In recent years, some important theoretical and experimental studies make it more and more apparent that the GP effects can be significant in molecular scattering.[65–75] In chemical reactions at thermal energies the GP effects were vanishingly small over a wide range of energies due to the fact that they wash out when a summation or average over all contributing partial waves. While, the situation changes dramatically in an energy regime where only a single partial wave contributes to the reactions, this is the case for ultra-cold chemical reactions in which manifest GP effects occur and it can be modulated by applying an external electric field allowing the possibility of quantum control of chemical reactions in the ultra-cold regime.[73–75] In 2014, S. K. Min *et al.* demonstrated that there exist cases where a nontrivial GP present in BO approximation does not have a topological counterpart in the exact electron-nuclear problem. But they emphasized that it is not known whether these cases are the majority or the exception. Since, in practice, we normally cannot solve the full electron-nuclear problem, it will be extremely important, but difficult, to find simple mathematical criteria by which one can know if a nonvanishing BO-Berry phase survives in the exact electron-nuclear treatment.[76]

The purpose of this work is to investigate the CIs and the associated GP effects among the five lowest singlet states of $Si(^1D) + H_2$ systems. The organization of the present article is as following. The details of the calculations are given in Sec. 2. The results are presented and discussed in Sec. 3. Finally, a brief summary is given in Sec. 4.

2 Theoretical approaches

2.1 *Ab initio* electronic structure calculations

The *ab initio* calculations presented in this work are performed with the MOLPRO suite of *ab initio* programs.[77] As the first step, the intersections are searched using the coupled-perturbed multi configuration self-consistent field (SA-CPMCSCF) method. For each calculation of locating the MECP between two electronic states, three vectors were evaluated at SA-CPMCSCF level: (1) non-adiabatic derivative coupling. (2) Gradient of the lower state. (3) Gradient of the upper state. Then, the internally contracted multireference configuration interaction (icMRCI) method was used for more sophisticated calculations of the single point energy. The icMRCI is a direct

MRCI procedure performed in an internally contracted configuration basis, and the MRCI wavefunctions include all single and double excitations relative to complete active space self-consistent field (CASSCF) reference functions.[78,79] In this work the icMRCI is employed to describe the most correlation energy of single and double electron excitations, and further correlation energy due to higher excitations is approximated by the Davidson correction (+Q).[80] The SA-CASSCF is a MCSCF method that the high level multireference SCF energies and wavefunctions for a series of ground and excited states is calculate by a state-averaged variational calculation. In essence, the SA approach included each of the states in question with equal weight and the configuration space is equivalent for all states.[81,82] In this work, the state-averaged complete active space self-consistent field (SA-CASSCF) calculation with 0.2, 0.2, 0.2, 0.2, 0.2 weighting on the five states is performed to obtain the orbitals for the icMRCI and SA-CPMCSCF calculations. In the SA-CASSCF calculation, the average energy of the five states, which asymptotically correlate with the five degenerate Si(^{1}D) states, is optimized. The active space consists of six electrons distributed among six orbitals (6e, 6o), which corresponds to all valence electrons and valence orbitals. All the calculations are performed in C_s symmetry, three lowest state of A′ symmetry and two lowest state of A″ symmetry are used for generating the internally contracted pairs in the icMRCI procedure. The basis set used is Dunning's correlation consistent polarized valence quadruple-zeta set augmented with diffuse functions[83–85] (aug-cc-pVQZ).

2.2 Characterization of the conical intersections

The topography of PES in the vicinity of a CI and the GP effect associated with the CI are discussed in the branching space of the CI. The branching space or g–h plane[26,51,86,87] is spanned by the orthonormal vectors $\vec{i} = \vec{g}/||\vec{g}||$ and $\vec{j} = \vec{h}/||\vec{h}||$, where $\vec{g}$ is the gradient difference, $\vec{h}$ is the derivative coupling vectors. The two vectors are determined by the analytic gradient technique in conjunction with the coupled-perturbed multi configuration self-consistent field SA-CPMCSCF method. Nuclear configurations in the branching space are characterized in terms of a set of natural polar coordinates in this plane, as shown in Fig. 1, $\vec{r}$ is the radial coordinate ($\vec{r} = x\cdot\vec{i} + y\cdot\vec{j}$), and φ is the angular coordinate or polar angle between $\vec{i}$ and $\vec{r}$. The CI is located at origin. Each r (we chose r = 0.01 : 0.01 : 0.2 in this work), together with the angular coordinate changing form 0 to 4π by the step 0.04π, define a trajectory of the nuclear configuration in the branching space. These nuclear configurations in the branching space are transformed into that in the Z-matrix before the electronic structure calculations. The PESs in branching space and the coefficient of the principal electron configuration of the related intersection electronic state are obtained from electronic structure calculations. Then, the double cone topographies of the PESs in the vicinity of the CI are evinced in the branching space, and the coefficient of the principal electron configuration of the related intersection electronic state along the motions of the nuclear configurations in the closed loop path around the CI in the two-dimensional specific branching space give rise to the GP effect.

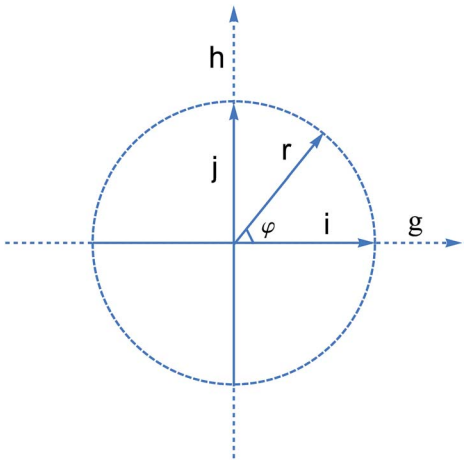

Fig. 1 Schematic illustration of the branching space of a CI. $\vec{i} = \vec{g}/||\vec{g}||$, $\vec{j} = \vec{h}/||\vec{h}||$.

3 Results and discussion

3.1 Energy correlation diagram

As an analog of methylene, SiH_2 radicals have the similar energy correlation diagram for the lowest singlet states $1^1A'$, $2^1A'$, $3^1A'$, $1^1A''$ and $2^1A''$, which correlate with the Si(^{1}D) + H_2 asymptote. The energy correlation diagram for the five singlet states is presented in Fig. 2. We can see that the $1^1A'$ and $1^1A''$ states are bounded relative to the Si + H_2 dissociation limit, the depth of them are 60.86 kcal mol^{-1} and 16.81 kcal mol^{-1}, respectively. While the $2^1A'$, $3^1A'$ and $2^1A''$ are above this limit. The resolutions of states of linear molecules into those of molecule in the C_{2v} or C_s symmetry, as shown in Table 1, indicate that the $^1A'$ and $^1A''$ states will become the degenerate Δ_g or Π_g pairs at linearity geometries. Our calculations demonstrate that the $1^1A'$, $1^1A''$ states and the $2^1A'$, $2^1A''$ states become the degenerate Δ_g and Π_g pairs, respectively, at linearity, and hence there are Renner–Teller coupling between them. The $1^1A'$ and $1^1A''$ states

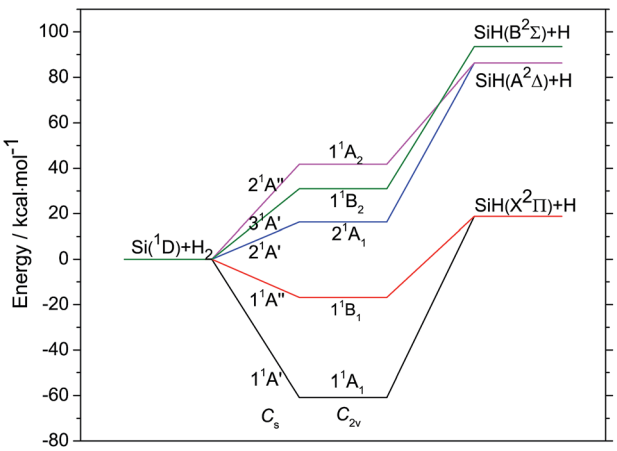

Fig. 2 Energy correlation diagram for the Si(^{1}D) + H_2 reactive system. It is determined by MRCI + Q method, the energies are relative to Si(^{1}D) + H_2 asymptote.

Table 1 Resolution of states of linear molecules into those of molecule in the C_{2v} or C_s symmetry

Linear molecule[a]	C_{2v} (z → y)	C_s ($\sigma_v \rightarrow \sigma$)
Σ_g^+	A_1	A′
Π_g	$A_2 + B_2$	A′ + A″
Δ_g	$A_1 + B_1$	A′ + A″

[a] The z axis in the linear case is assumed to lie in the internuclear direction.

degenerate in the product asymptote and they are correlated with SiH($X^2\Pi$) + H products, the $2^1A'$ and $2^1A''$ states degenerate in the product asymptote and they are correlated with SiH($X^2\Delta$) + H products. The reaction Si(^1D) + H_2 → SiH($X^2\Pi$) + H have a significant endothermicity of 18.81 kcal mol^{-1}, which is very different from the most researched insertion-type reactions X + H_2 → HX + H (X = C, N, O, S) with more or less exothermicity.[88,89]

The geometries of minima for the five singlet states of SiH_2 radical are summarized in Table 2 and compared with the available experimental and theoretical values.[8,12,15,23] The equilibrium SiH distances and the equilibrium HSiH angles of SiH_2 $1^1A'$, $1^1A''$, $2^1A'$ and $3^1A'$ states agree well with the available experimental or theoretical values. To our knowledge, it is the first time that the geometry and the relative energy of SiH_2 $2^1A''$ are reported in detail.

3.2 Conical intersections

The CIs relative to the five lowest singlet states of Si(^1D) + H_2 asymptote are investigated systematically. The intersections covers CIs between $1^1A'$ and $2^1A'$ states, CIs between $2^1A'$ and $3^1A'$ states, at linear H–Si–H geometries; CIs between $1^1A'$ and $2^1A'$ states, CIs between $2^1A'$ and $3^1A'$ states, at linear Si–H–H geometries; CIs between $1^1A''$ and $2^1A''$ states, CIs between $2^1A'$ and $3^1A'$ states at C_{2v} geometries. The intersection seams of CIs are searched. Minimum energy crossing point (MECP) is an important point of an intersection seam. The energies and geometries of the MECPs on each intersection seams are reported in Table 3. The topographies of the PESs in the branching space of the MECPs and the GP effects associated with the MECPs are discussed. All these intersections are classified in terms of the symmetries of SiH_2 geometries and will be discussed in detail below.

Table 2 Equilibrium geometries and their relative energies of the lowest five singlet states of SiH_2. The energies are relative to the Si(^1D) + H_2 asymptote. Bond length in bohr, bond angle in degrees, and energies in kcal mol^{-1}

	Methods	R_{SiH}	∠HSiH	Energies
$SiH_2(1^1A')$	MRCI + Q[a]	2.871	92.2	−60.86
	MRCI[b]	2.870	92.2	
	expt[c]	2.874	92.1	
	expt[d]	2.865	92.1	
	expt[e]	2.861	92.1	
$SiH_2(1^1A'')$	MRCI + Q[a]	2.817	122.8	−16.81
	MRCI[b]	2.816	122.7	
	expt[c]	2.806	122.0	
	expt[d]	2.810	123.0	
$SiH_2(2^1A')$	MRCI + Q[a]	2.777	165.1	16.34
	MRCI[b]	2.776	164.8	
$SiH_2(3^1A')$	MRCI + Q[a]	3.160	180.0	36.37
	MRCI[b]	3.115	180.0	
$SiH_2(2^1A'')$	MRCI + Q[a]	2.582	64.4	41.80

[a] This work. [b] From ref. 8. [c] From ref. 12. [d] From ref. 15. [e] From ref. 23.

3.2.1 Conical intersections at linear H–Si–H geometries.

The intersection seam between the $1^1A'$ and $2^1A'$ states and the energies along the seam are shown in Fig. S1(a) of the ESI.† The MECP on this seam locates at the geometry with $R_{SiH_1} = 3.056$ bohrs and $R_{SiH_2} = 3.485$ bohrs, as shown in Table 3, and the energy of this MECP is 33.37 kcal mol^{-1}. This MECP actually determines the special barrier hindering the H–Si–H bond fission to yield the SiH product and induce the barrier for H + SiH collinear hydrogen exchange reaction. The topographies of the PESs in the branching space of this MECP are shown in Fig. 3(a), it clearly indicates that this MECP is actually related to four ($1^1A'$, $2^1A'$, $1^1A''$, $2^1A''$) states, so as the seam it locates on. When it comes to the linear geometry, the $^1A'$, $1^1A''$ states and the $2^1A'$, $2^1A''$ states become degenerate pairs respectively. The four states are degenerate at the MECP geometry and forming the double cone. The two lower cones ($1^1A'$ and $1^1A''$ states) surfaces in this region are in lack of the bound-states and the two upper cones ($2^1A'$ and $2^1A''$) surfaces form a local minima in this region. It should notice that there is a CI which belongs to the intersection seam between $2^1A'$ and $3^1A'$ on the upper solid surface which is corresponding to the $2^1A'$ state, and with the nuclear configuration passing through this point in the negative direction of $\vec{g}$, the $2^1A'$ and $2^1A''$ become non-degenerate states.

The intersection seam between the $2^1A'$ and $3^1A'$ states and the energies along the seam are shown in Fig. S1(b) of the ESI.† The MECP on this seam locates at the geometry with $R_{SiH_1} = 3.160$ bohrs $R_{SiH_2} = 3.160$ bohrs, which happen to be a C_{2v} geometry, as shown in Table 3, and the energy of this MECP is 36.37 kcal mol^{-1}. The topographies of the branching space PESs in the vicinity of this MECP are show in Fig. 3(b), it shows that this MECP is actually related to three ($2^1A'$, $3^1A'$, $2^1A''$) states, so as the seam it located on. With that the nuclear configuration moving in the negative direction of $\vec{g}$, the components of the Π_g pair are $2^1A'$ and $2^1A''$ states before the nuclear configuration reaching the MECP, and switch into $3^1A'$ and $2^1A''$ states after that. The upper cone of this branching space PESs is also bounded in this region, while the lower cone is lack of bound-states in the vicinity of the MECP. It is obvious that there is a CI which belongs to the intersection seam between the $1^1A'$ and $2^1A'$ states on the lower cone, and the PES in the vicinity of this CI is bounded.

It has been mentioned that there is a CI point which belongs to the intersection seam between the $2^1A'$ and $3^1A'$ states on the branching space PES in the vicinity of the MECP between $1^1A'$ and $2^1A'$ states, conversely there is a CI point which belongs to the intersection seam between the $1^1A'$ and $2^1A'$ states on the branching space PES in the vicinity of the MECP between $2^1A'$ and $3^1A'$ states. In order to clarify the GP effects of these CIs, we

Table 3 The geometries and relative energies of the minimum energy crossing points on the intersection seams among different states of the $Si(^1D) + H_2$ reactive system. The energies are relative to the $Si(^1D) + H_2$ asymptote, bond length in bohr, bond angle HSiH in degree and energy in kcal mol^{-1}, $R_{SiH_2} > R_{SiH_1}$ at linear Si–H–H geometries

Classification	Electronic states	Geometries of MECPs	Energies of MECPs
H–Si–H	$1^1A'(1^1A'')$–$2^1A'(2^1A'')$	$R_{SiH_1} = 3.056$, $R_{SiH_2} = 3.485$	33.37
H–Si–H	$2^1A'(2^1A'')$–$3^1A'(2^1A'')$	$R_{SiH_1} = 3.160$, $R_{SiH_2} = 3.160$	36.37
Si–H–H	$1^1A'(1^1A'')$–$2^1A'(2^1A'')$	$R_{SiH_1} = 3.578$, $R_{HH} = 1.952$	24.06
Si–H–H	$2^1A'(2^1A'')$–$3^1A'(2^1A'')$	$R_{SiH_1} = 4.210$, $R_{HH} = 1.370$	11.13
C_{2v}	$1^1A''$–$2^1A''$	$R_{SiH} = 3.165$, $\angle HSiH = 68.45$	21.60
C_{2v}	$2^1A'$–$3^1A'$	$R_{SiH} = 2.855$, $\angle HSiH = 60.68$	118.13

extract the linear H–Si–H geometries out of the geometries of SiH_2 that distributing in the branching spaces. The intersection seams and the lines consisting of linear H–Si–H geometries extracted from the corresponding MECP branching spaces are shown in Fig. 4. The MECPs are the centers of the extracted linear geometries lines and other linear geometries with different r ($r = 0 : 0.01 : 0.2$) are symmetrically distributed with the MECPs. It shows that the cross point between the line that consists of the linear geometries extracted from the branching space of MECP between $1^1A'$ and $2^1A'$ states and the intersection seam that between the $2^1A'$ and $3^1A'$ states is located in the region with $0.09 < r < 0.10$ and $\varphi = \pi$ in the branching space of the MECP between $1^1A'$ and $2^1A'$ states. The cross point between the line that consists of linear geometries extracted from the branching space of the MECP between $2^1A'$ and $3^1A'$ states and the intersection seam that between $1^1A'$ and $2^1A'$ states is located in the region with $0.10 < r < 0.11$ and $\varphi = \pi$ in the branching space of the MECP between $2^1A'$ and $3^1A'$ states.

It had been mentioned that with the nuclear configurations completing a closed path encircling a CI odd number of times, the sign of the corresponding real adiabatic electronic wavefunctions will change, which called GP effect. In this work the GP effects are discussed in the branching spaces of corresponding MECPs. Fig. 5 shows the coefficients of principal configuration of the related electronic states change along the closed paths consisting of two loops encircling the MECPs with different r ($r = 0.01 : 0.01 : 0.2$), and it present the GP effects in the title system. Three dimension representation of the GP effects are shown in Fig. S2 of the ESI.†

As for the $1^1A'$ electronic state corresponding to the lower cone of the branching space PES of $1^1A'$ and $2^1A'$ states, all of the nuclear configuration paths with different r encircle only one CI, that is the MECP between $1^1A'$ and $2^1A'$ states, so the signs of the electronic wavefunctions corresponding to the paths with different r will change with the nuclear configurations completing the first closed loop path and change back to their original states with the second one, $C(\varphi) = -C(\varphi + 2\pi)$, and this is shown in Fig. 5(a).

The $2^1A'$ electronic state corresponding to the upper cone of the branching space PES of $1^1A'$ and $2^1A'$ involves two CIs, one is the MECP between $1^1A'$ and $2^1A'$ states and another is a common CI belonging to the intersection seam between $2^1A'$ and $3^1A'$ states and it is located in the region with $0.09 < r < 0.10$ in this branching space. If $r \leq 0.09$, the closed nuclear configuration paths encircle only one CI, and the signs of the corresponding electronic wavefunctions will change with the nuclear configurations completing the closed loop path and change back to their original states with the second one, $C(\varphi) = -C(\varphi + 2\pi)$. While, if $r \geq 0.10$, the closed paths encircle two CI points, and the signs of the corresponding electronic wavefunctions will not change with the nuclear configurations completing any number of loops, $C(\varphi) = C(\varphi + 2\pi)$, and this is shown in Fig. 5(b).

The $2^1A'$ electronic state corresponding to the lower cone of the branching space PES of $2^1A'$ and $3^1A'$ states, involves two CIs, one is the MECP between $2^1A'$ and $3^1A'$ states and another is a common CI belonging to the intersection seam between $1^1A'$ and $2^1A'$ states and it is located in the region with $0.10 < r < 0.11$ in this branching space. If $r \leq 0.10$, the closed nuclear configuration paths encircle only one CI, and the signs of the electronic wavefunctions corresponding to the paths with different r will change with the nuclear configurations completing the first loop and change back to their original state after the second one, $C(\varphi) = -C(\varphi + 2\pi)$. While, if $r \geq 0.11$, the closed paths encircle two CIs, and the signs of the corresponding electronic wavefunctions will not change with the nuclear configurations completing any number of loops. This is shown in Fig. 5(c).

As for the $3^1A'$ electronic state corresponding to the upper cone of the branching space PES of $2^1A'$ and $3^1A'$ states, all of the nuclear configuration paths with different r encircle only one CI that is the MECP between $2^1A'$ and $3^1A'$, so the signs of the electronic wavefunctions corresponding to the paths with different r will change with the nuclear configurations completing the first loop and change back to their original states with the second one, $C(\varphi) = -C(\varphi + 2\pi)$. This is shown in Fig. 5(d).

3.2.2 Conical intersections at linear Si–H–H geometries. The intersection seam between the $1^1A'$ and $2^1A'$ states at the linear Si–H–H geometries and the energies along the seam are shown in Fig. S1(c) of the ESI.† The MECP on this seam is located at the geometry with $R_{SiH_1} = 3.578$ bohrs $R_{HH} = 1.952$ bohrs, as shown in Table 3, and the energy of this MECP is 24.06 kcal mol^{-1}. This MECP actually determines the special barrier for the $Si(^1D)$ collinearly approaching to the H_2. The topography of the branching space PES in the vicinity of this MECP is shown in Fig. 3(c), like the intersection at linear H–Si–H geometries, this MECP is actually related to four ($1^1A'$, $2^1A'$, $1^1A''$, $2^1A''$)

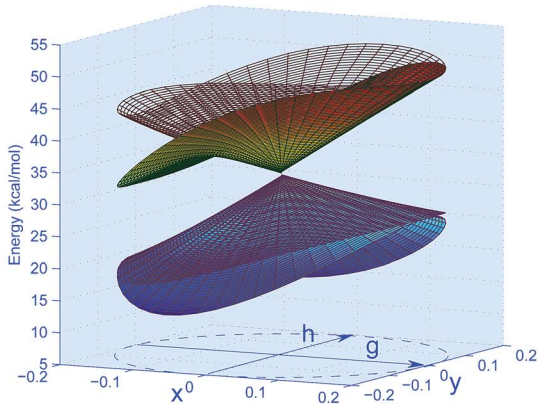

(a) The $1^1A'(1^1A'')$–$2^1A'(2^1A'')$ intersection at linear H-Si-H geometries. The $1^1A'$ and $2^1A'$ correspond to solid surfaces, the $1^1A''$ and $2^1A''$ correspond to mesh surfaces.

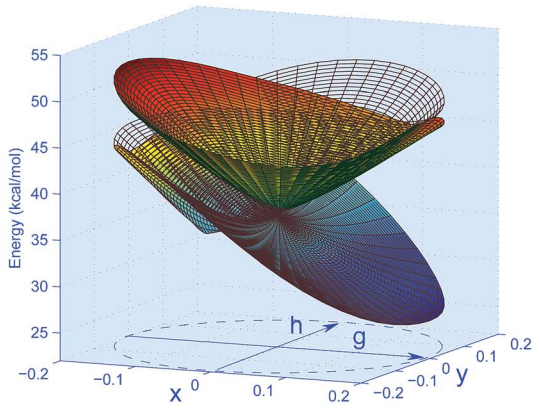

(b) The $2^1A'(2^1A'')$–$3^1A'(2^1A'')$ intersection at linear H-Si-H geometries. The $2^1A'$ and $3^1A'$ correspond to solid surfaces, the $2^1A''$ correspond to mesh surfaces.

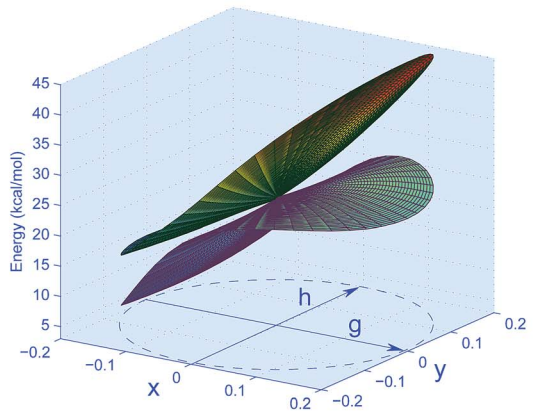

(c) The $1^1A'(1^1A'')$–$2^1A'(2^1A'')$ intersection at linear Si-H-H geometries.

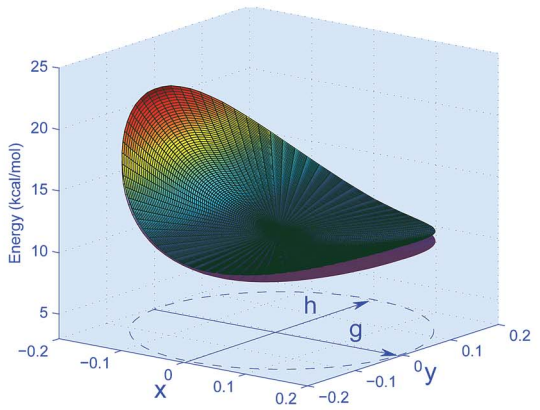

(d) The $2^1A'(2^1A'')$–$3^1A'(2^1A'')$ intersection at linear Si-H-H geometries.

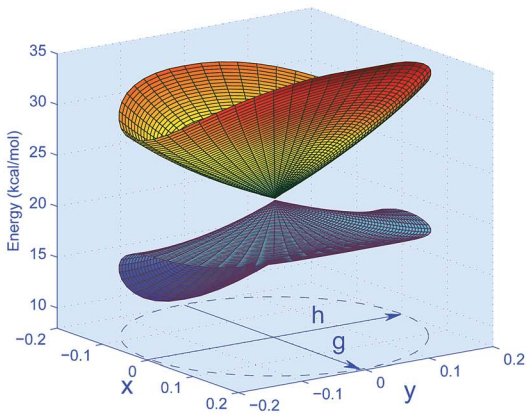

(e) The $1^1A''$–$2^1A''$ intersection at C_{2v} geometries.

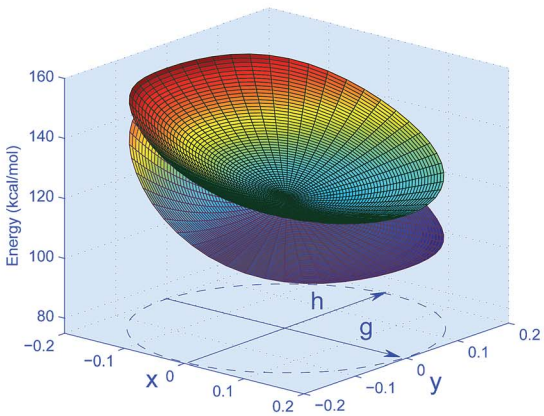

(f) The $2^1A'$–$3^1A'$ intersection at C_{2v} geometries.

Fig. 3 The topography of potential energy surfaces in the branching space of the minimum energy crossing points of the intersections at linear H–Si–H geometries (a and b), linear Si–H–H geometries (c and d) and C_{2v} geometries (e and f). The corresponding nuclear configurations are distributed in the branching space with $r = 0 : 0.01 : 0.2$ and $\varphi = 0 : 0.04\pi : 2\pi$. The energies are relative to Si(^{1}D) + H_2 asymptote.

states, so as the seam it located on. The ^{1}A′, 1^1A″ states and the 2^1A′, 2^1A″ states become degenerate pairs, respectively, at linear geometries. Since that even at non-linear geometries the 1^1A′, 1^1A″ states and the 2^1A′, 2^1A″ states are very close to each other in energy, it seem that they are keep being degenerate pairs in all the MECP branching space region with $r < 0.2$ which is the

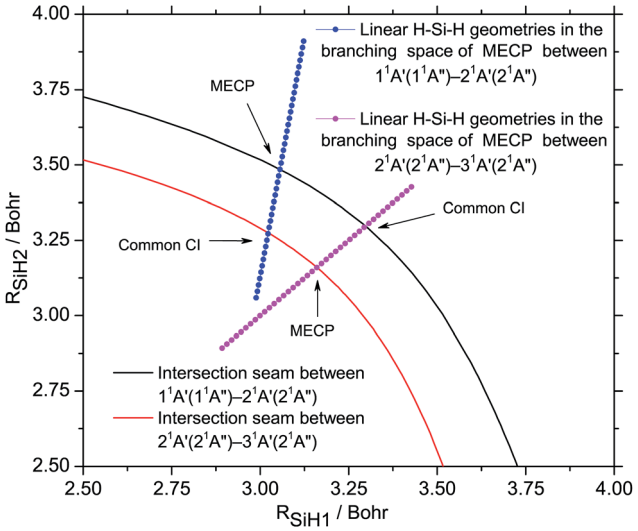

Fig. 4 The intersection seams at linear H–Si–H geometries and the line of linear H–Si–H geometries in the branching space (r = 0 : 0.01 : 0.2, $\varphi = 0 : 0.04\pi : 2\pi$) of MECP of corresponding seams.

largest r defined in this work. The four states are degenerate at the MECP geometry and forming the double cone. It is necessary to mention that there is a CI which belongs to the intersection seam between $2^1A'$ and $3^1A'$ states on the edge of the upper cone, as the relevant electronic states in this region are very close with each other in energies, it is not as obvious as that at linear H–Si–H geometries, but it will be clarified in the below paragraphs.

The intersection seam between the $2^1A'$ and $3^1A'$ states and the energies along the seam are shown in Fig. S1(d) of the ESI.† The MECP on this seam is located at the geometry with $R_{SiH_1} = 4.210$ bohrs and $R_{HH} = 1.370$ bohrs, as shown in Table 3, and the energy of this MECP is 11.13 kcal mol^{-1}. The topography of the branching space PES in the vicinity of this MECP is shown in Fig. 3(d), it should be similar with the intersection between the $2^1A'$ and $3^1A'$ states at the linear H–Si–H geometries that this MECP involve three ($2^1A'$, $3^1A'$, $2^1A''$) states, so as the seam it located on. With the nuclear configuration moving in the negative direction of $\vec{g}$, the components of the Π_g pair are $2^1A'$ and $2^1A''$ before the nuclear configuration reaching the MECP, and switch into $3^1A'$ and $2^1A''$ after that, but this is less obvious compared with that at the linear H–Si–H geometries since that the three relevant states in this region are very close to each other in energy.

The intersection seams and the lines consisting of linear Si–H–H geometries extracted from the MECP branching spaces are shown in Fig. 6. The MECPs are the centers of the extracted linear geometries lines and other linear geometries with different r ($r = 0 : 0.01 : 0.2$) are symmetrically distributed with the MECPs. It shows that the cross point between the line that consists of linear geometries extracted from the branching space of the MECP between $1^1A'$ and $2^1A'$ states and the intersection seam that between $2^1A'$ and $3^1A'$ states is located in the region with $0.17 < r < 0.18$ and $\varphi = \pi$ in this branching space. There is not a cross point between the line that consists of linear geometries extracted from the branching space of the MECP between $2^1A'$ and $3^1A'$ states and the intersection seam that between $1^1A'$ and $2^1A'$ states.

As for the $1^1A'$ electronic state corresponding to the lower cone of the branching space PES of $1^1A'$ and $2^1A'$ states, all of the nuclear configuration paths with different r encircle only one CI that is the MECP between $1^1A'$ and $2^1A'$ states, so the signs of the electronic wavefunctions corresponding to the nuclear configuration paths with different r will change with the nuclear configurations completing the first closed loop path and change back to their original states with the second one, $C(\varphi) = -C(\varphi + 2\pi)$, and this is shown in Fig. 5(e).

The $2^1A'$ electronic state corresponding to the upper cone of the branching space PES of $1^1A'$ and $2^1A'$ states involves two CIs, one is the MECP between $^1A'$ and $2^1A'$ states and another is a common CI belonging to the intersection seam between $2^1A'$ and $3^1A'$ states located in the region with $0.17 < r < 0.18$ and $\varphi = \pi$ in this branching space. If $r \leq 0.17$, the closed loop paths of nuclear configurations encircle only one CI, so the signs of the electronic wavefunctions corresponding to the nuclear configurations paths with different r will change with the nuclear configurations completing the first closed loop and change back to their original states with the second one, $C(\varphi) = -C(\varphi + 2\pi)$. While, if $r \geq 0.18$, the closed loop paths encircle two CIs, and the corresponding electronic wavefunctions will not change sign with the nuclear configurations completing any number of loops, $C(\varphi) = C(\varphi + 2\pi)$. That is shown in Fig. 5(f). All of this confirm that there is a CI on edge the upper cone of branching space PES of $1^1A'$ and $2^1A'$ states, and the CI is one point of intersection seam between $2^1A'$ and $3^1A'$ states.

As for both of the $2^1A'$ and $3^1A'$ electronic states corresponding to the lower cone and the upper cone of the branching space PES of $2^1A'$ and $3^1A'$ states, respectively, all of the nuclear configuration paths with different r encircle only one CI that is the MECP between $2^1A'$ and $3^1A'$ states. So, the signs of the electronic wavefunctions corresponding to the nuclear configuration paths with different r will change with the nuclear configurations completing the first closed loop and change back to their original states after the second one, $C(\varphi) = -C(\varphi + 2\pi)$, and this is shown in Fig. 5(g) and (h).

3.2.3 Conical intersections at C_{2v} geometries. Two intersection seams are found at C_{2v} geometries of the title system. The intersection seam between the $1^1A''$ and $2^1A''$ states and the energies along the seam are shown in Fig. S1(e) of the ESI.† The MECP on this seam is located at the geometry with $R_{SiH} = 3.165$ bohrs and $\angle HSiH = 68.45$ degree, as shown in Table 3, and the energy of this MECP is 21.60 kcal mol^{-1}. The intersection seam between the $2^1A'$ and $3^1A'$ states is shown in Fig. S1(f) of the ESI.† The MECP on this seam locates at the geometry with $R_{SiH} = 2.855$ bohrs and $\angle HSiH = 60.68$ degree, as seen from Table 3, and the energy of this MECP is 118.13 kcal mol^{-1}. The topographies of the branching space PESs in the vicinity of the MECP between $1^1A''$ and $2^1A''$ states and that in the vicinity of the MECP between the $2^1A'$ and $3^1A'$ states are shown in Fig. 3(e) and (f). Both of the branching space PESs have the double cone structure. It seems that there are not any other CIs being involved in the two branching space PESs within $r \leq 0.2$.

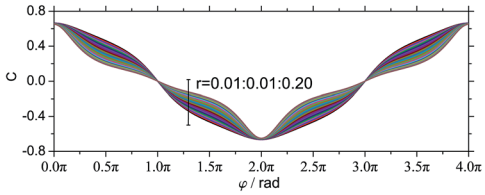

(a) The $1^1A'$ state in the $1^1A'(1^1A'')$–$2^1A'(2^1A'')$ intersection at linear H-Si-H geometries .

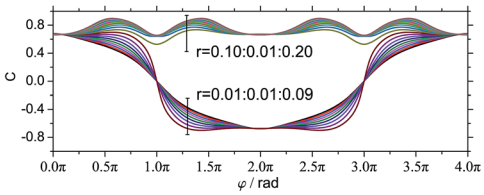

(b) The $2^1A'$ state in the $1^1A'(1^1A'')$–$2^1A'(2^1A'')$ intersection at linear H-Si-H geometries.

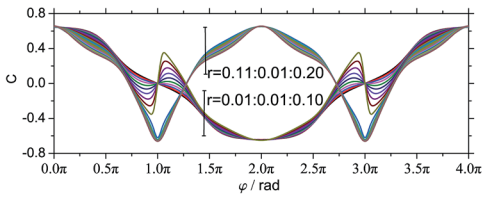

(c) The $2^1A'$ state in the $2^1A'(2^1A'')$–$3^1A'(2^1A'')$ intersection at linear H-Si-H geometries.

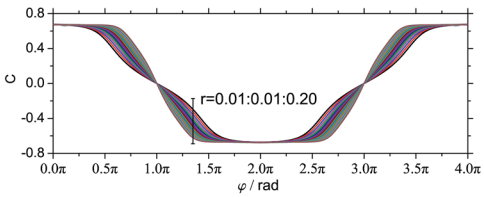

(d) The $3^1A'$ state in the $2^1A'(2^1A'')$–$3^1A'(2^1A'')$ intersection at linear H-Si-H geometries.

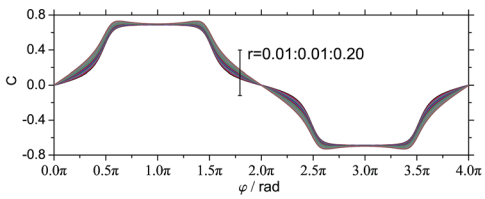

(e) The $1^1A'$ state in the $1^1A'(1^1A'')$–$2^1A'(2^1A'')$ intersection at linear Si-H-H geometries.

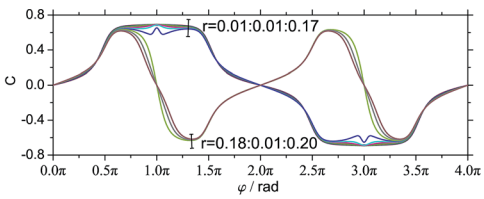

(f) The $2^1A'$ state in the $1^1A'(1^1A'')$–$2^1A'(2^1A'')$ intersection at linear Si-H-H geometries.

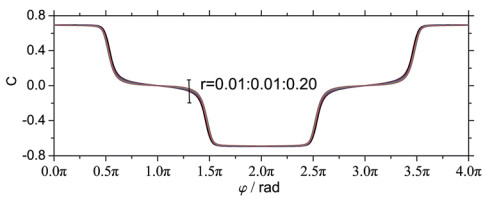

(g) The $2^1A'$ state in the $2^1A'(2^1A'')$–$3^1A'(2^1A'')$ intersection at linear Si-H-H geometries.

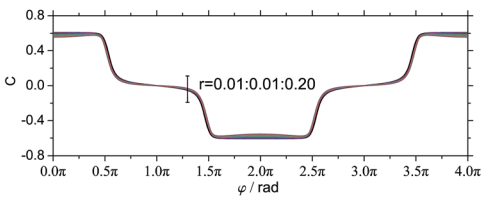

(h) The $3^1A'$ state in the $2^1A'(2^1A'')$–$3^1A'(2^1A'')$ intersection at linear Si-H-H geometries.

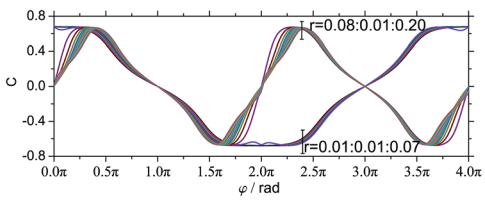

(i) The $1^1A''$ state in the $1^1A''$–$2^1A''$ intersection at C_{2v} geometries.

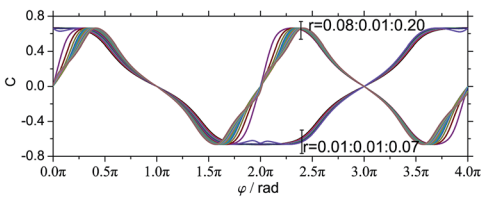

(j) The $2^1A''$ state in the $1^1A''$–$2^1A''$ intersection at C_{2v} geometries.

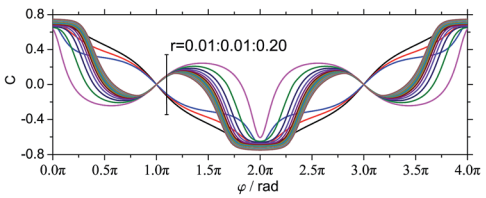

(k) The $2^1A'$ state in the $2^1A'$–$3^1A'$ intersection at C_{2v} geometries.

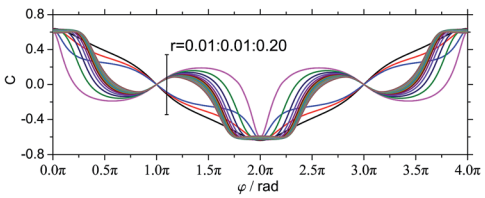

(l) The $3^1A'$ state in the $2^1A'$–$3^1A'$ intersection at C_{2v} geometries.

Fig. 5 Coefficient of the principal electron configuration of the related intersection electronic state along the paths correspond to $r = 0.01 : 0.01 : 0.2$ and $\varphi = 0 : 0.04\pi : 4\pi$ in the branching space of minimum energy crossing points of intersection in Si(^{1}D) + H_2 system.

The GP effects associated with the MECP between $1^1A''$ and $2^1A''$ states are shown in Fig. 5(i) and (j). As for both of the $1^1A''$ state and the $2^1A''$ state, if $r \leq 0.07$, the signs of the corresponding electronic wavefunctions will change with the nuclear configuration completing the first loop and change back to their original states with the second one, $C(\varphi) = -C(\varphi + 2\pi)$.

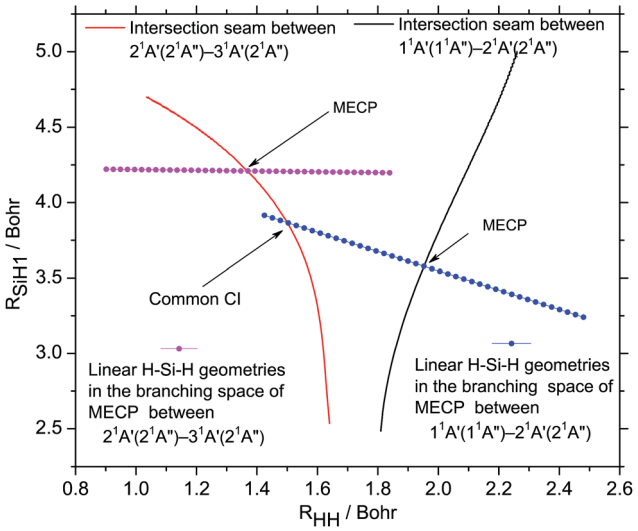

Fig. 6 The intersection seams at linear Si–H–H geometries and the line of linear Si–H–H geometries in the branching space (r = 0 : 0.01 : 0.2, φ = 0 : 0.04π : 2π) of MECP of the corresponding seams.

While, if $r \geq 0.08$, the corresponding electronic wavefunctions will not change sign with the nuclear configurations completing any number of loops, $C(\varphi) = C(\varphi + 2\pi)$. It indicate that there is a CI on lower and upper cones of the branching space PESs in the vicinity of MECP between $1^1A''$ and $2^1A''$ states in the region with $0.07 < r < 0.08$, respectively. While this is not apparent in the topography of the branching space PES. We reason that there are some other electronic states that have not been taken into consideration in this work intersecting with the $1^1A''$, $2^1A''$ states.

The GP effects associated with the MECP between $2^1A'$ and $3^1A'$ states are shown in Fig. 5(k) and (l). As for both of the $2^1A'$ electronic and $3^1A'$ state, the signs of the corresponding electronic wavefunctions will change with the nuclear configurations completing the first closed loop and change back to its original states after the second one, $C(\varphi) = -C(\varphi + 2\pi)$. It demonstrate that all of the nuclear configuration paths with different r encircle only one CI that is the MECP of intersection seam between $2^1A'$ and $3^1A'$ states. It is true that except the MECP there is not any other CI in the vicinity of the MECP within $r \leq 0.2$ in the branching space.

4 Conclusions

CIs among the $1^1A'$, $2^1A'$, $3^1A'$, $1^1A''$, $2^1A''$ states of the title system are investigated using the CASSCF or MRCI method. Finally several CI seams at the linear H–Si–H, linear Si–H–H and C_{2v} geometries are determined. The CI seams at the linear H–Si–H, Si–H–H geometries are accompanied by Renner–Teller coupling. The CI seams between $1^1A'$ and $2^1A'$ states actually involve four states: the $1^1A'$, $1^1A''$ Renner–Teller coupling pair and the $2^1A'$, $2^1A''$ Renner–Teller coupling pair. The CI seams between $2^1A'$ and $3^1A'$ states simultaneously involve $2^1A''$ state, for which the components of the Renner–Teller coupling pair are $2^1A'$ and $2^1A''$ before the MECP, and switch into $3^1A'$ and $2^1A''$ after the MECP.

The geometries and energies of the MECPs on these CI seams are reported, in particular, the MECP of CI seam between $1^1A'$ and $2^1A'$ states at the linear H–Si–H geometries is in the linear H–SiH dissociation direction and it induce the barrier for H + SiH collinear hydrogen exchange reaction with a height of 22.45 kcal mol^{-1}. The MECP of CI seam between $1^1A'$ and $2^1A'$ states at the linear Si–H–H geometries is located on the minimum energy reaction path of the Si(^{1}D) + H_2 collinear abstraction reaction, and it determines the energy barrier with a height of 24.06 kcal mol^{-1}.

The topographies of PESs in the vicinities of the MECPs are represented in their branching spaces. The double cone features of the branching space PESs around the MECPs at the linear H–Si–H geometries and the C_{2v} SiH_2 geometries are obvious. While, the double cone features of the branching space PESs around the MECPs at the linear Si–H–H geometries are subtle, as the related electronic states are close to each other in energy. In spite of that, the GP effects associated with the MECPs corroborate that the MECPs at the linear Si–H–H geometries are actually CIs, as with that at the linear H–Si–H and C_{2v} SiH_2 geometries.

The GP effects of these MECPs are demonstrated. The GP effects associated with the MECPs of intersection between $1^1A''$, $2^1A''$ states at the C_{2v} geometries indicate that there are some other electronic states that have not been taken into consideration in this work intersecting with the $1^1A''$, $2^1A''$ states.

We hope that this work will be helpful to providing intuitive understanding of the CIs and GP effects, and will contribute to the researches about diabatic dynamics with CIs and GP effects in the title system.

Acknowledgements

This work is supported by the National Natural Science Foundation of China (No. 21473218), the Chinese Ministry of Science and Technology (No. 2013CB834601), and the Beijing National Laboratory for Molecular Sciences (No. 20140160, 20150158) and Chinese Academy of Sciences.

References

1 J. M. Jasinski and J. O. Chu, *J. Chem. Phys.*, 1988, **88**, 1678–1687.
2 M.-D. Su, *J. Am. Chem. Soc.*, 2002, **124**, 12335–12342.
3 M. Denk, J. C. Green, N. Metzler and M. Wagner, *J. Chem. Soc., Dalton Trans.*, 1994, **16**, 2405–2410.
4 S. Koseki and M. S. Gordon, *J. Mol. Spectrosc.*, 1987, **123**, 392–404.
5 R. Escribano and A. Campargue, *J. Chem. Phys.*, 1998, **108**, 6249–6257.
6 M. Wang, X. Sun and W. Bian, *J. Chem. Phys.*, 2008, **129**, 084309.
7 J. Cao, Z. Zhang, C. Zhang, K. Liu, M. Wang and W. Bian, *Proc. Natl. Acad. Sci. U. S. A.*, 2009, **106**, 13180–13185.
8 I. Dubois, G. Herzberg and R. D. Verma, *J. Chem. Phys.*, 1967, **47**, 4262–4263.

9 D. E. Milligan and M. E. Jacox, *J. Chem. Phys.*, 1970, **52**, 2594–2608.
10 B. Wirsam, *Chem. Phys. Lett.*, 1972, **14**, 214–216.
11 Y. Apeloig, R. Pauncz, M. Karni, R. West, W. Steiner and D. Chapman, *Organometallics*, 2003, **22**, 3250–3256.
12 I. Dubois, *Can. J. Phys.*, 1968, **46**, 2485–2490.
13 I. Dubois, G. Duxbury and R. N. Dixon, *J. Chem. Soc., Faraday Trans. 2*, 1975, **71**, 799–806.
14 G. Duxbury, A. Alijah and R. R. Trieling, *J. Chem. Phys.*, 1993, **98**, 811–825.
15 C. Yamada, H. Kanamori, E. Hirota, N. Nishiwaki, N. Itabashi, K. Kato and T. Goto, *J. Chem. Phys.*, 1989, **91**, 4582–4586.
16 J. W. Thoman, J. I. Steinfeld, R. I. McKay and A. E. W. Knight, *J. Chem. Phys.*, 1987, **86**, 5909–5917.
17 M. Fukushima, S. Mayama and K. Obi, *J. Chem. Phys.*, 1992, **96**, 44–52.
18 J. Thoman and J. Steinfeld, *Chem. Phys. Lett.*, 1986, **124**, 35–38.
19 M. Fukushima and K. Obi, *J. Chem. Phys.*, 1994, **100**, 6221–6227.
20 M. Nakajima, A. Kawai, M. Fukushima and K. Obi, *Chem. Phys. Lett.*, 2002, **364**, 99–107.
21 H. Ishikawa, Y. Muramoto and N. Mikami, *J. Mol. Spectrosc.*, 2002, **216**, 90–97.
22 S. N. Yurchenko, P. R. Bunker, W. P. Kraemer and P. Jensen, *Can. J. Chem.*, 2004, **82**, 694–708.
23 Y. Muramoto, H. Ishikawa and N. Mikami, *J. Chem. Phys.*, 2005, **122**, 154302.
24 I. Tokue, K. Yamasaki and S. Nanbu, *J. Chem. Phys.*, 2005, **122**, 144307.
25 I. Tokue, K. Yamasaki and S. Nanbu, *J. Chem. Phys.*, 2006, **124**, 114308.
26 D. R. Yarkony, *Acc. Chem. Res.*, 1998, **31**, 511–518.
27 T. J. Martinez, *Nature*, 2010, **467**, 412–413.
28 S. Matsika and P. Krause, *Annu. Rev. Phys. Chem.*, 2011, **62**, 621–643.
29 G. A. Worth and L. S. Cederbaum, *Annu. Rev. Phys. Chem.*, 2004, **55**, 127–158.
30 M. R. Manaa and D. R. Yarkony, *J. Chem. Phys.*, 1992, **97**, 715–717.
31 A. Perveaux, P. J. Castro, D. Lauvergnat, M. Reguero and B. Lasorne, *J. Phys. Chem. Lett.*, 2015, **6**, 1316–1320.
32 D. R. Yarkony, *Rev. Mod. Phys.*, 1996, **68**, 985–1013.
33 F. Bouakline, S. C. Althorpe and D. Peláez Ruiz, *J. Chem. Phys.*, 2008, **128**, 124322.
34 J. P. Villabona-Monsalve, R. Noria, S. Matsika and J. Peón, *J. Am. Chem. Soc.*, 2012, **134**, 7820–7829.
35 Y. Asano, A. Murakami, T. Kobayashi, A. Goldberg, D. Guillaumont, S. Yabushita, M. Irie and S. Nakamura, *J. Am. Chem. Soc.*, 2004, **126**, 12112–12120.
36 H. Kang, K. T. Lee, B. Jung, Y. J. Ko and S. K. Kim, *J. Am. Chem. Soc.*, 2002, **124**, 12958–12959.
37 F. Bernardi, S. De, M. Olivucci and M. A. Robb, *J. Am. Chem. Soc.*, 1990, **112**, 1737–1744.
38 J. Brazard, L. A. Bizimana, T. Gellen, W. P. Carbery and D. B. Turner, *J. Phys. Chem. Lett.*, 2016, **7**, 14–19.
39 C. Schnedermann, M. Liebel and P. Kukura, *J. Am. Chem. Soc.*, 2015, **137**, 2886–2891.
40 G. J. Halász, Á. Vibók and L. S. Cederbaum, *J. Phys. Chem. Lett.*, 2015, **6**, 348–354.
41 D. Polli, P. Altoe, O. Weingart and K. M. Spillane, *Nature*, 2010, **467**, 440–443.
42 J. G. Atchity, K. Ruedenberg and A. Nanayakkara, *Theor. Chem. Acc.*, 1997, **96**, 195–204.
43 H. J. Wörner, J. B. Bertrand, B. Fabre and J. Higuet, *Science*, 2011, **334**, 208–212.
44 B. Zhou, C. Zhu, Z. Wen, Z. Jiang, J. Yu, Y.-P. Lee and S. H. Lin, *J. Chem. Phys.*, 2013, **139**, 154302.
45 S. Y. Grebenshchikov and R. Borrelli, *J. Phys. Chem. Lett.*, 2012, **3**, 3223–3227.
46 M. R. Manaa, *J. Chem. Phys.*, 2000, **112**, 8789–8793.
47 G. Chaban, M. S. Gordon and D. R. Yarkony, *J. Phys. Chem. A*, 1997, **101**, 7953–7959.
48 M. S. Gordon, V.-A. Glezakou and D. R. Yarkony, *J. Chem. Phys.*, 1998, **108**, 5657–5659.
49 A. Vibók, G. J. Halósz, T. Vèrteśi, S. Suhai, M. Baer and J. P. Toennies, *J. Chem. Phys.*, 2003, **119**, 6588–6596.
50 D. R. Yarkony, *J. Chem. Phys.*, 1996, **104**, 2932–2939.
51 N. Matsunaga and D. R. Yarkony, *J. Chem. Phys.*, 1997, **107**, 7825–7838.
52 X. Liu, W. Bian, X. Zhao and X. Tao, *J. Chem. Phys.*, 2006, **125**, 074306.
53 M. V. Berry, *Proc. R. Soc. A*, 1984, **392**, 45–57.
54 L. Fu, C. L. Kane and E. J. Mele, *Phys. Rev. Lett.*, 2007, **98**, 106803.
55 D. Xiao, M.-C. Chang and Q. Niu, *Rev. Mod. Phys.*, 2010, **82**, 1959–2007.
56 Y. Aharonov and D. Bohm, *Phys. Rev.*, 1959, **115**, 485–491.
57 J. W. Zwanziger, M. Koenig and A. Pines, *Annu. Rev. Phys. Chem.*, 1990, **41**, 601–646.
58 I. G. Ryabinkin and A. F. Izmaylov, *Phys. Rev. Lett.*, 2013, **111**, 220406.
59 G. Herzberg and H. C. Longuet-Higgins, *Discuss. Faraday Soc.*, 1963, **35**, 77–82.
60 C. A. Mead, *Rev. Mod. Phys.*, 1992, **64**, 51–85.
61 B. E. Applegate, T. A. Barckholtz and T. A. Miller, *Chem. Soc. Rev.*, 2003, **32**, 38–49.
62 B. K. Kendrick and R. T. Pack, *J. Chem. Phys.*, 1997, **106**, 3519–3539.
63 B. K. Kendrick, *Phys. Rev. Lett.*, 1997, **79**, 2431–2434.
64 D. Babikov, B. K. Kendrick, P. Zhang and K. Morokuma, *J. Chem. Phys.*, 2005, **122**, 044315.
65 B. K. Kendrick, *J. Chem. Phys.*, 2001, **114**, 8796–8819.
66 B. K. Kendrick, *J. Chem. Phys.*, 2003, **118**, 10502–10522.
67 B. K. Kendrick, *J. Phys. Chem. A*, 2003, **107**, 6739–6756.
68 J. C. Juanes-Marcos and S. C. Althorpe, *J. Chem. Phys.*, 2005, **122**, 204324.
69 J. C. Juanes-Marcos, S. C. Althorpe and E. Wrede, *Science*, 2005, **309**, 1227–1230.
70 S. C. Althorpe, *J. Chem. Phys.*, 2006, **124**, 084105.
71 J. C. Juanes-Marcos, S. C. Althorpe and E. Wrede, *J. Chem. Phys.*, 2007, **126**, 044317.

72 J. Jankunas, M. Sneha, R. N. Zare, F. Bouakline and S. C. Althorpe, *J. Chem. Phys.*, 2013, **139**, 144316.
73 J. Hazra, B. K. Kendrick and N. Balakrishnan, *J. Phys. Chem. A*, 2015, **119**, 12291–12303.
74 B. K. Kendrick, J. Hazra and N. Balakrishnan, *Nat. Commun.*, 2015, **6**, 7918.
75 B. K. Kendrick, J. Hazra and N. Balakrishnan, *Phys. Rev. Lett.*, 2015, **115**, 153201.
76 S. K. Min, A. Abedi, K. S. Kim and E. K. U. Gross, *Phys. Rev. Lett.*, 2014, **113**, 263004.
77 H. J. Werner, P. J. Knowles, G. Knizia, F. R. Manby and M. Schutz, *MOLPRO, Version 2010.1*, a Package of Ab Initio programs, see http://www.molpro.net.
78 H.-J. Werner and P. J. Knowles, *J. Chem. Phys.*, 1988, **89**, 5803–5814.
79 P. J. Knowles and H.-J. Werner, *Chem. Phys. Lett.*, 1988, **145**, 514–522.
80 S. R. Langhoff and E. R. Davidson, *Int. J. Quantum Chem.*, 1974, **8**, 61–72.
81 H.-J. Werner and P. J. Knowles, *J. Chem. Phys.*, 1985, **82**, 5053–5063.
82 P. J. Knowles and H.-J. Werner, *Chem. Phys. Lett.*, 1985, **115**, 259–267.
83 T. H. Dunning, *J. Chem. Phys.*, 1989, **90**, 1007–1023.
84 R. A. Kendall, T. H. Dunning and R. J. Harrison, *J. Chem. Phys.*, 1992, **96**, 6796–6806.
85 D. E. Woon and T. H. Dunning, *J. Chem. Phys.*, 1993, **98**, 1358–1371.
86 B. C. Hoffman and D. R. Yarkony, *J. Chem. Phys.*, 2000, **113**, 10091–10099.
87 F. Sicilia, L. Blancafort, M. J. Bearpark and M. A. Robb, *J. Phys. Chem. A*, 2007, **111**, 2182–2192.
88 F. J. Aoiz, L. Banares and V. J. Herrero, *J. Phys. Chem. A*, 2006, **110**, 12546–12565.
89 H. Guo, *Int. Rev. Phys. Chem.*, 2012, **31**, 1–68.